Characterization of ferroelectric NaxK1-xNbO3 system films prepared by pulsed laser deposition

Materials Transactions, Vol. 49, No. 9 (2008) pp. 2076 to 2081

Characterization of Ferroelectric $Na_xK_{1-x}NbO_3$ System Films Prepared by Pulsed Laser Deposition

Fengping Lai[1], Rong Tu[1], Takashi Goto[1] and Jingfeng Li[2]

[1]*Institute for Materials Research, Tohoku University, Sendai 980-8577, Japan*
[2]*State Key Laboratory of New Ceramics and Fine Processing, Department of Materials Science and Engineering, Tsinghua University, Beijing 100084, P. R. China*

Ferroelectric $Na_xK_{1-x}NbO_3$ (NKN) films were prepared on quartz and $Pt/SrTiO_3(100)$ substrates by pulsed laser deposition. The effects of composition and preparation conditions on the crystal structure and ferroelectricity of the NKN films were investigated by changing the Na content (x), substrate temperature (T_{sub}), oxygen partial pressure (P_{O_2}), target-to-substrate distance ($D_{t\text{-}s}$) and laser energy density (E_L). The permittivity values of the NKN films were 390 to 520 at room temperature and 100 kHz, showing a maximum at $x = 0.5$. The maximum remnant polarization value was $8.2 \times 10^{-2}\,C\,m^{-2}$ at $x = 0.5$. [doi:10.2320/matertrans.MRA2008116]

(Received April 8, 2008; Accepted June 5, 2008; Published July 16, 2008)

Keywords: *sodium potassium niobate film, pulse laser deposition, ferroelectricity*

1. Introduction

The $NaNbO_3$-$KNbO_3$ solid solution system is a promising lead-free ferroelectric and piezoelectric material and thus great effort has been made to increase its ferroelectric and piezoelectric performance.[1,2] According to the phase diagram for the solid solution of the $Na_xK_{1-x}NbO_3$ (NKN) system, a morphotropic phase boundary (MPB) separating two orthorhombic ferroelectric phases exists at an x of around 0.5.[3] Near this MPB composition, the dielectric constant and piezoelectric constant are the highest[4,5] with the smallest coercive field (E_c).[6] Saito *et al.* reported that $Na_{0.5}K_{0.5}NbO_3$-based sintered bodies had a large piezoelectric coefficient (d_{33}), with a comparable value to that of commercial $Pb(Zr,Ti)O_3$ (PZT).[7,8]

NKN and NKN-based thin films have potential applications for non-volatile ferroelectric random access memories (FRAM) and ferroelectric actuators and devices in microelectromechanical system (MEMS). $Na_{0.5}K_{0.5}NbO_3$ films have been prepared by several routes, including pulsed laser deposition (PLD),[9,10] magnetron sputtering,[11,12] metal-organic chemical vapor deposition (MOCVD)[13,14] and sol-gel.[15,16]

Pulsed laser deposition has been widely applied for preparation of many kinds of thin films due to several advantages, i.e., stoichiometric transfer of compositions from source to film, growth from a high energy beam resulting in high crystallinity and inherent simplicity for the growth of multilayered structures.[17] $Na_{0.5}K_{0.5}NbO_3$ thin films were first prepared by Cho *et al.* using pulsed laser deposition.[18] Kim *et al.* prepared a highly oriented $Na_{0.5}K_{0.5}NbO_3$ film by pulsed laser deposition, the piezoelectric constant of which was comparable to that of epitaxially grown PZT film by pulsed laser deposition.[19]

However, no study on NKN films with various compositions has been reported. In this work, NKN films were prepared by pulsed laser deposition, and the effects of preparation conditions on the crystal structure and the electrical properties of the films were investigated.

2. Experimental

Starting materials of Na_2CO_3, K_2CO_3 and Nb_2O_5 powders were mixed in the nominal composition of $Na_xK_{1-x}NbO_3$ with x changing from 0.2 to 0.8, pressed into pellets with diameter (Φ) of 15 mm and height (H) of 3 mm and then calcined at 1173 K for 14.4 ks. The pellets were sintered by spark plasma sintering (SPS) at 1323 K for $x = 0.2$ to 0.6 and at 1373 K for $x = 0.8$ for 600 s in a vacuum and then annealed at 1123 K for 36 ks in air.

NKN films were prepared on quartz glass and $Pt/SrTiO_3(100)$ substrates by pulsed laser deposition. Hereafter, various compositions of NKN films are expressed as xNKN, where x represents the nominal composition ($Na_xK_{1-x}NbO_3$) of the targets. A third harmonic wavelength of a Q-switch pulsed Nd:YAG laser (Spectron Laser System SL805, $\lambda = 355$ nm, pulse duration of 15 ns and repetition of 10 Hz) was used as the laser source. Deposition parameters are summarized in Table 1.

Amorphous quartz plates ($12 \times 10 \times 0.5$ mm) and $SrTiO_3(100)$ single crystal wafers ($10 \times 10 \times 0.5$ mm) with a Pt bottom electrode were used as substrates. The target and substrate stage were rotated at 12 rpm in converse directions. Films were deposited at a vacuum (10^{-7} Pa) and different oxygen partial pressures (P_{O_2}) ranging from 2.67 to 26.7 Pa.

Table 1 Deposition parameters for NKN films prepared by pulsed laser deposition.

Targets	NKN pellets ($x = 0.2$ to 0.8, Φ 15 mm, H 3 mm)
Substrate	Quartz glass, STO (100) single crystal
Substrate temperature (T_{sub})	723–973 K
Deposition ambient	Vacuum (10^{-7} Pa) Oxygen partial pressure, P_{O_2} (2.67–26.7 Pa)
Distance between target and substrates ($D_{t\text{-}s}$)	40–70 mm
Laser energy density (E_L)	$2–7.5 \times 10^4\,J\,m^{-2}$
Deposition time	3.6–14.4 ks

The substrate temperature (T_{sub}) was changed from 723 to 973 K. The distance between the target and the substrate ($D_{t\text{-}s}$) was changed stepwise from 45 to 70 mm. The power density of the laser output (E_L) was controlled in a range from 2 to 7.5×10^4 J m^{-2}.

The crystal structure was examined by X-ray diffraction (Rigaku, RAD-2C). To determine the lattice constants of the targets and the films, X-ray step scanning was employed. The thickness was measured by a profilemeter (Taylor-Hobson Talystep). The composition was studied by electron probe microanalysis (EPMA, JEOL JXA-8621MX). The surface morphology was observed by scanning electron microscopy (SEM, Hitachi S-3100H). The dielectric properties were measured in air by an AC impedance analyzer (Hewlett Packard 4194) in a frequency (f) range of 10^2 to 10^7 Hz from room temperature to 773 K. The polarization–electric field (P–E) hysteresis loops were measured by a ferroelectric test system (FCE-1, TOYO Corp., Japan) at a frequency (f) of 10 kHz at room temperature.

3. Results and Discussion

Figure 1 shows the effect of x on the XRD patterns of NKN films at $P_{O_2} = 10$ Pa, $T_{sub} = 973$ K, $D_{t\text{-}s} = 60$ mm and $E_L = 3.8 \times 10^4$ J m^{-2} for 7.2 ks. Perovskite structures were obtained in NKN films with different compositions, which were the powder diffraction of $KNbO_3$ (JCPDS #32-0822) and $NaNbO_3$ (JCPDS #33-1270). A small amount of second phases of $K_4Nb_6O_{17}$ (Orthorhombic, $a = 0.783$, $b = 3.321$ and $c = 0.646$ nm) and $K_2Nb_8O_{21}$ (Orthorhombic, $a = 1.25$, $b = 3.75$ and $c = 0.396$ nm) was contained at 0.2NKN and 0.8NKN, respectively. The $NaNbO_3$-$KNbO_3$ system is a pseudo-binary solid solution system in the whole range and all targets were of perovskite structure in a single phase. Second phases observed in the NKN films near the two end members could have been caused by the volatilization of Na and K, which is a common problem encountered in the preparation of compounds containing alkali metal elements.[20,21] In addition, slight changes in stoichiometry (both on the Na-rich and the K-rich side) easily lead to the formation of second phases.[22]

NKN films with different compositions had similar dense microstructures with particulates, showing little dependence on composition.

The average compositions of NKN films measured by EPMA were almost in agreement with that of the targets. The difference of Na/(Na+K) and (Na+K)/Nb ratios between the NKN films and targets was less than 10%.

The structure of $NaNbO_3$ and $KNbO_3$ crystals is orthorhombic at RT with lattice parameters of $a = 0.5568$ nm, $b = 1.552$ nm and $c = 0.5504$ nm, and $a = 0.5695$ nm, $b = 0.5721$ nm and $c = 0.3973$ nm, respectively. To compare lattice parameters between NKN films and bulk crystals, the lattice parameters were transformed into a pseudo-cubic structure through relations of $a_c = a/\sqrt{2}$, $b_c = b/\sqrt{2}$ and $c_c = c$.[23] Figure 2 depicts the pseudo-cubic lattice parameters of the NKN targets and films prepared at $T_{sub} = 973$ K and $P_{O_2} = 10$ Pa for 7.2 ks on quartz glass substrates. The lattice parameters of both targets and NKN films decreased with increasing Na content. A transition of slope in lattice parameters occurred at $x = 0.4$ to 0.6 for both targets and films, owing to the MPB composition of $NaNbO_3$–$KNbO_3$ system. The lattice parameters of the NKN films were smaller than those of the targets, which might have been due to compressive stress generated during the pulsed laser deposition and/or cooling process. Film compressive stress has been reported to arise due to a variety of different mechanisms, including differential thermal contraction, island coalescence, grain growth, grain boundary diffusion, competitive columnar growth and high-energy particle bombardment.[24] Since the thermal expansion coefficient of quartz is smaller than that of NKN films, the smaller lattice parameters of NKN films can not be explained by the difference in thermal expansion, but may result from

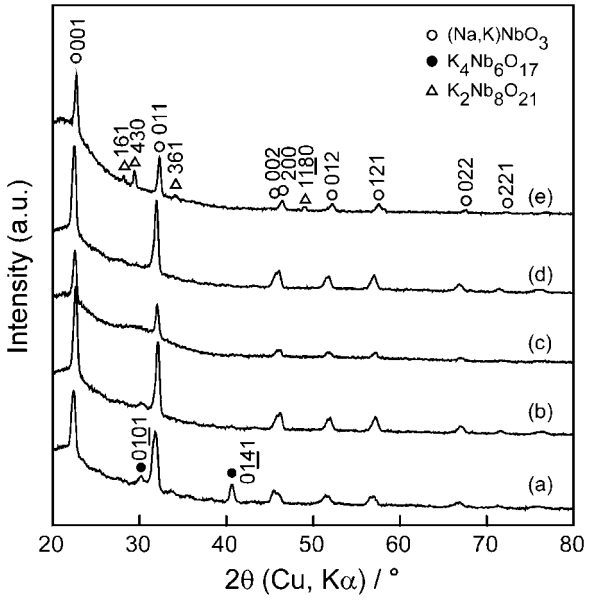

Fig. 1 Effect of x on XRD patterns of NKN films deposited on quartz glass at $x = 0.2$ (a), 0.4 (b), 0.5 (c), 0.6 (d) and 0.8 (e) at $T_{sub} = 973$ K, $P_{O_2} = 10$ Pa, $D_{t\text{-}s} = 60$ mm and $E_L = 3.8 \times 10^4$ J m^{-2} for 7.2 ks.

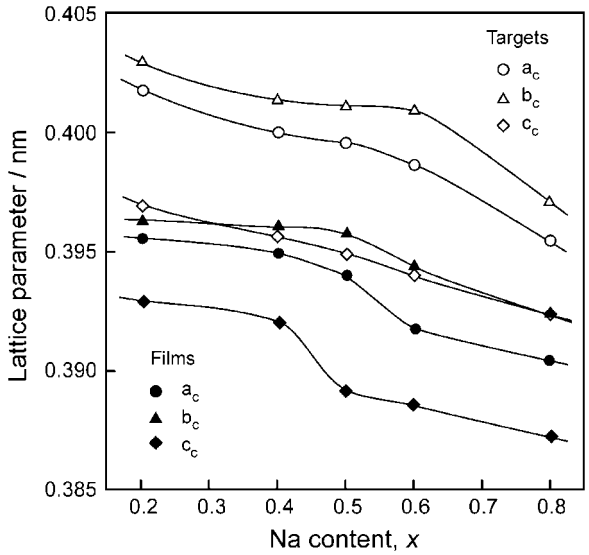

Fig. 2 Effect of x on the pseudo-cubic lattice parameters a_c, b_c and c_c of the NKN targets and films (subscript c means pseudo-cubic).

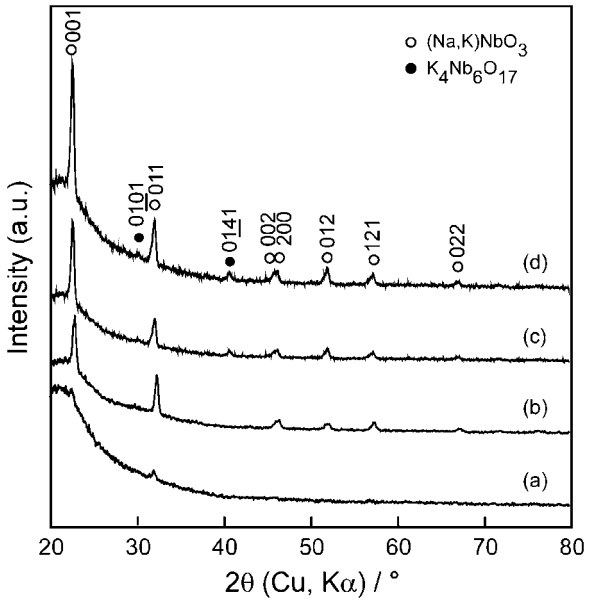

Fig. 3 Effect of T_{sub} on XRD patterns of 0.5NKN films prepared on quartz glass at $T_{sub} = 723$ (a), 873 (b), 923 (c) and 973 K (d) at $P_{O_2} = 10$ Pa, $D_{t\text{-}s}$ of 50 mm and $E_L = 3.8 \times 10^4$ J m^{-2} for 3.6 ks.

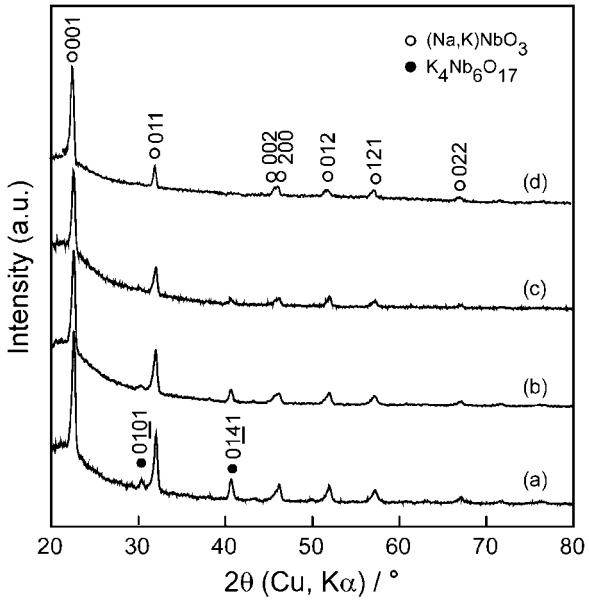

Fig. 5 Effect of P_{O_2} on XRD patterns of 0.5NKN films prepared on quartz glass at vacuum (a), $P_{O_2} = 2.67$ (b), 10 (c) and 26.7 Pa (d) at $T_{sub} = 973$ K, $D_{t\text{-}s} = 50$ mm and $E_L = 3.8 \times 10^4$ J m^{-2} for 3.6 ks.

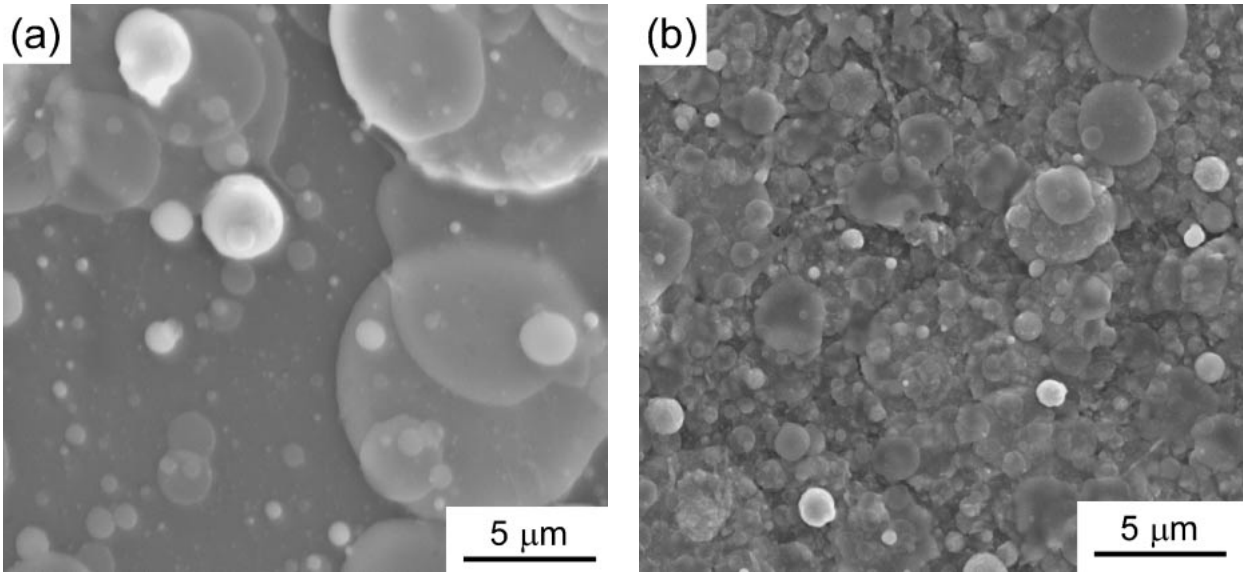

Fig. 4 Effect of T_{sub} on microstructures of 0.5NKN films prepared on quartz glass at $T_{sub} = 723$ (a) and 973 K (b) at $P_{O_2} = 10$ Pa, $D_{t\text{-}s} = 50$ mm and $E_L = 3.8 \times 10^4$ J m^{-2} for 3.6 ks.

the stress generated during the pulsed laser deposition process. Some stoichiometric deviation or defects in the NKN films may also be associated with the smaller lattice parameters.[25)]

The effect of deposition parameters, such as T_{sub}, P_{O_2}, $D_{t\text{-}s}$ and E_L, on the crystal structure and microstructure of NKN films will be described later, taking $x = 0.5$ as an example.

Figure 3 shows the effect of T_{sub} on the XRD patterns of 0.5NKN films prepared at $P_{O_2} = 10$ Pa, $D_{t\text{-}s} = 50$ mm and $E_L = 3.8 \times 10^4$ J m^{-2} for 3.6 ks. A perovskite structure of 0.5NKN film was identified at each T_{sub}. The (001) peak of 0.5NKN film became significant with increasing T_{sub}, showing (001) orientational growth. A small amount of the second phase of $K_4Nb_6O_{17}$ was detected at $T_{sub} = 923$ and 973 K.

Figure 4 shows the effect of T_{sub} on the microstructure of 0.5NKN films. The 0.5NKN film showed a micro-sized particulate microstructure with a relative flat matrix at $T_{sub} = 723$ K and a dense particulate microstructure at $T_{sub} = 973$ K. The stacking density of the particulates increased with increasing T_{sub}, which was associated with decreasing particulate size. This indicates that the adhesion between the substrate and the ablated species increased at higher T_{sub}. There was no obvious existence of a second phase at high T_{sub} from surface morphology observation.

Figure 5 shows the effect of P_{O_2} on the XRD patterns of the 0.5NKN films prepared at $T_{sub} = 923$ K, $D_{t\text{-}s} = 50$ mm

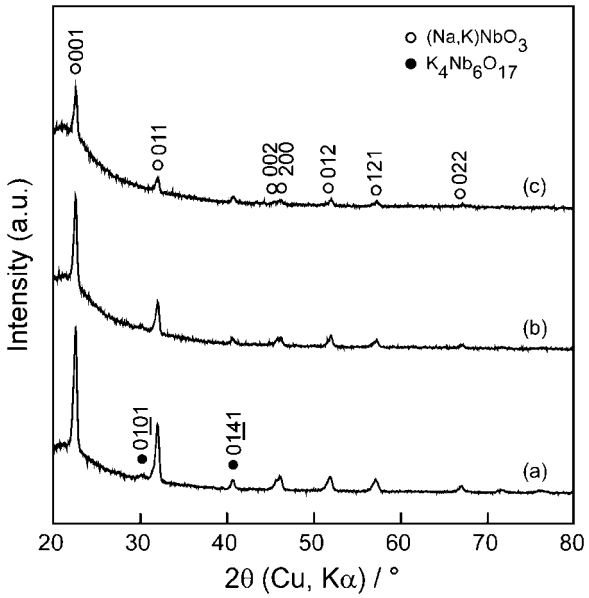

Fig. 6 Effect of $D_{t\text{-}s}$ on XRD patterns of 0.5NKN films prepared on quartz glass at $D_{t\text{-}s} = 50$ (a), 60 (b) and 70 mm (c) at $T_{sub} = 973$ K, P_{O_2} of 10 Pa and $E_L = 3.8 \times 10^4$ J m^{-2} for 3.6 ks.

and $E_L = 3.8 \times 10^4$ J m^{-2} for 3.6 ks. In a vacuum ($P = 10^{-7}$ Pa), a small amount of the second phase of $K_4Nb_6O_{17}$ appeared. The peaks of $K_4Nb_6O_{17}$ and 0.5NKN films decreased with increasing P_{O_2}. The intensity ratio of (001) to (011) of 0.5NKN film ($I_{NKN\text{-}001}/I_{NKN\text{-}011}$) increased from 2.1 in a vacuum to 5.3 at $P_{O_2} = 26.7$ Pa, while it was 0.67 for the 0.5NKN target. This implies that the (001) orientation of 0.5NKN films is preferred at higher P_{O_2}. A similar effect of P_{O_2} on the preferred orientation of $Na_{0.5}K_{0.5}NbO_3$ films has been reported for $Pt_{80}Ir_{20}$ and SiO_2(native oxide)/Si(111) substrates by Cho *et al.*[10] In their work, second phases of $K_2Nb_8O_{21}$ and $K_2Nb_4O_{11}$ were identified at $P_{O_2} = 1.33$ Pa. The formation of alkaline-poor niobates by pulsed laser deposition at a low P_{O_2} may be caused by the high volatility of Na and K. At high P_{O_2} (~53.2 Pa), the present 0.5NKN films were in a single phase and were highly (001)-oriented ($I_{NKN\text{-}001}/I_{NKN\text{-}011} = 60$), showing a tendency similar to that reported by Cho *et al.*[10]

Figure 6 shows the effect of $D_{t\text{-}s}$ on the XRD patterns of 0.5NKN films prepared at 973 K, $P_{O_2} = 10$ Pa and $E_L = 3.8 \times 10^4$ J m^{-2}. The intensities of the second phase ($K_4Nb_6O_{17}$) and perovskite 0.5NKN film decreased with increasing $D_{t\text{-}s}$. A moderate distance and a longer deposition time were appropriate to obtain 0.5NKN films.

The microstructures of 0.5NKN films did not show much difference under different P_{O_2} and $D_{t\text{-}s}$, except for a decreasing stacking density of the particulates. The specific effects of P_{O_2} and $D_{t\text{-}s}$ were interrelated. The more collisions which occurred between the laser-produced plume and the background gas, the lower the number of ablated species which arrived at the surface of substrates.

Figure 7 shows the effect of E_L on the surface microstructure of 0.5NKN films prepared at $T_{sub} = 973$ K, $P_{O_2} = 10$ Pa and $D_{t\text{-}s} = 50$ mm. 0.5NKN films had a dense microstructure with particulates at $E_L = 5 \times 10^4$ J m^{-2} and a granular microstructure with micron-sized particulates at $E_L = 3.8 \times 10^4$ J m^{-2}. The amount of particulates decreased significantly with decreasing E_L. At $E_L < 2.5 \times 10^4$ J m^{-2}, a dense microstructure with a grain size of 500 nm and a few particulates were observed. The deposition rates of 0.5NKN films dramatically decreased from about 1.4 to 0.07×10^{-10} m s^{-1} with decreasing E_L from 5 to 2×10^4 J m^{-2}. Moreover, the XRD patterns of 0.5NKN films turned to be amorphous when E_L decreased to 2×10^4 J m^{-2}, partly due to the slow deposition rate. $D_{t\text{-}s}$ of 40 mm and E_L of 2.5×10^4 J m^{-2} were found to be effective to achieve an increase in the deposition rate to 0.6×10^{-10} m s^{-1} with clear perovskite XRD peaks and only slight particulate generation, as shown in Fig. 7(d).

Figure 8 shows the temperature dependence of permittivity at 100 kHz for NKN films prepared on a Pt/STO(100) substrate at $T_{sub} = 973$ K, $P_{O_2} = 10$ Pa and $D_{t\text{-}s} = 60$ mm for 7.2 ks. The permittivity continuously increased with increasing temperature and exhibited peaks around 680 K. The Curie temperature (T_c) slightly increased from 670 to 700 K with decreasing x from 0.8 to 0.2, slightly less than those of sintered bodies reported by Egerton *et al.*[19] The permittivity peak value of 5000 was obtained for 0.5NKN films, which was larger than those of 1200 and 2500 for $Na_{0.5}K_{0.5}NbO_3$ films prepared by Khartsev *et al.* using RF-sputtering and pulsed laser deposition, respectively.[26] The permittivity value of 5000 obtained in the present study is the highest thus far reported in the literature.

Figure 9 shows the hysteresis loops of NKN films prepared on Pt/STO (100) substrates at $T_{sub} = 973$ K, $P_{O_2} = 10$ Pa and $D_{t\text{-}s} = 60$ mm for 7.2 ks. Well-saturated hysteresis loops were observed at $f = 10$ kHz under an electrical field of 5×10^6 V m^{-1} at room temperature. The remnant polarization (P_r) reached the highest value of 8.2×10^{-2} C m^{-2} for 0.5NKN. The coercive field (E_c) of NKN films varied from 1.24 to 1.57×10^6 V m^{-1}. The value of E_c was the highest at 0.6NKN, with a slight dependence on the composition. These E_c values were smaller than that of 2×10^6 V m^{-1} of the c-axis-oriented NKN films prepared by Cho *et al.*[10]

Figure 10 demonstrates the permittivity (ε') and remnant polarization (P_r) of NKN films as a function of Na content at room temperature. The ε' of NKN films at $f = 100$ kHz ranged from 390 to 520 and showed the maximum value in 0.5NKN film. The permittivity of NKN films had a compositional dependence similar to that of NKN ceramics. The peak permittivity of NKN ceramics was observed at $x = 0.5$ by Chu *et al.*[27] and around $x = 0.4$ to 0.6 by Zhang *et al.*[5] Several groups have reported the permittivity of NKN films. Table 2 summarizes the permittivity of NKN films prepared by various processes, indicating rather small values of 37 by RF magnetron sputtering[28] and 545 by aerosol deposition.[29] High permittivity values above 500 have been reported for epitaxial and (001)-oriented 0.5NKN films,[10,11] whereas the non-oriented 0.5NKN film in the present study showed a relatively high value. To date various compositions of NKN films have been prepared, but only the composition of 0.5NKN film has been focused on in the literature. This paper is the first to report the composition dependence of ε' and P_r, and the study herein reported achieved the highest ε' of NKN film to date.

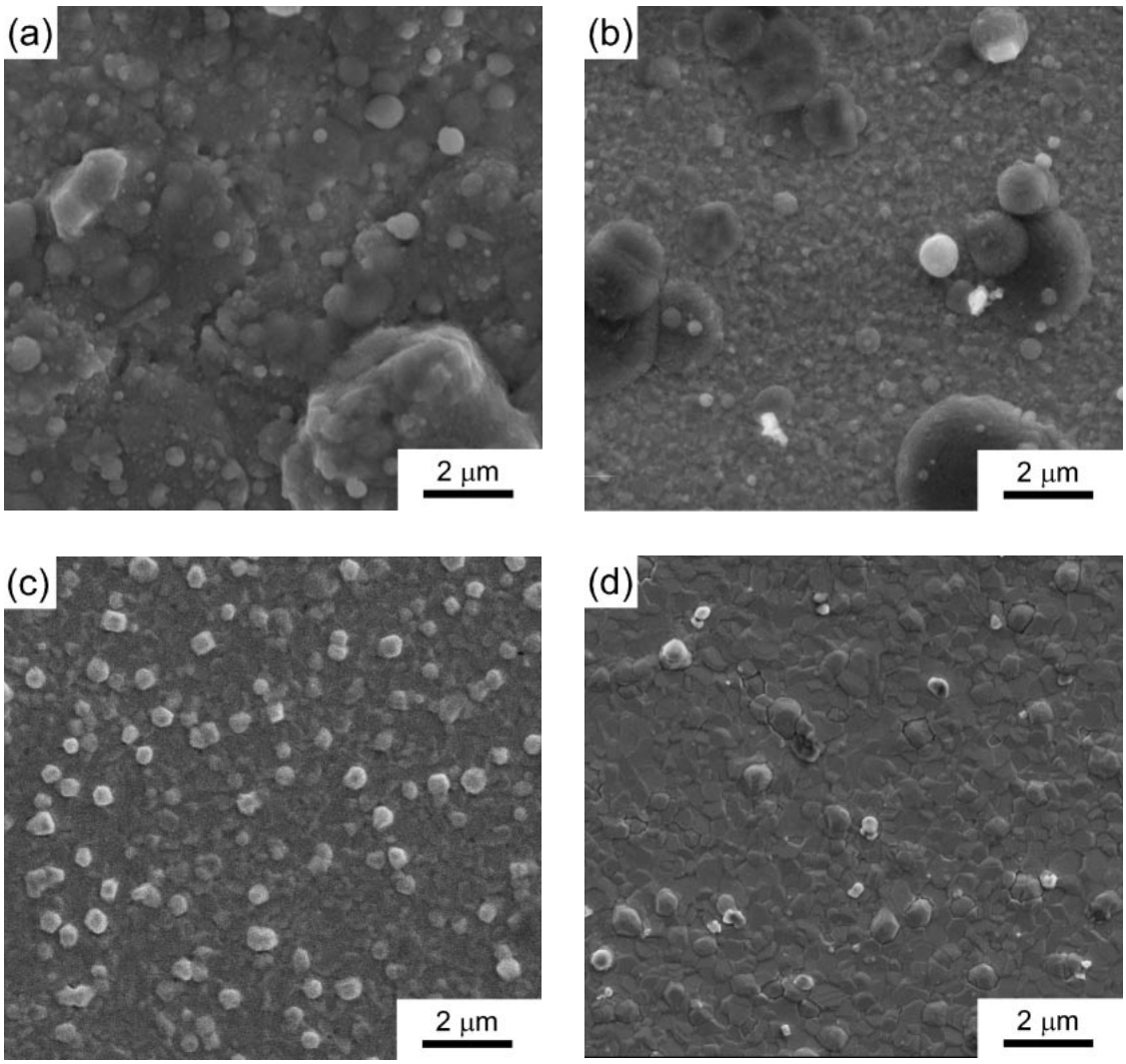

Fig. 7 Effect of E_L on microstructures of 0.5NKN films prepared on quartz glass at $E_L = 5 \times 10^4\,J\,m^{-2}$ and $D_{t\text{-}s} = 60\,mm$ for 7.2 ks (a), $3.8 \times 10^4\,J\,m^{-2}$ and $D_{t\text{-}s} = 60\,mm$ for 3.6 ks (b), $2 \times 10^4\,J\,m^{-2}$ and $D_{t\text{-}s} = 60\,mm$ for 30.4 ks (c) and $2.5 \times 10^4\,J\,m^{-2}$ and $D_{t\text{-}s} = 40\,mm$ for 3.6 ks (d), $T_{sub} = 973\,K$, $P_{O_2} = 10\,Pa$.

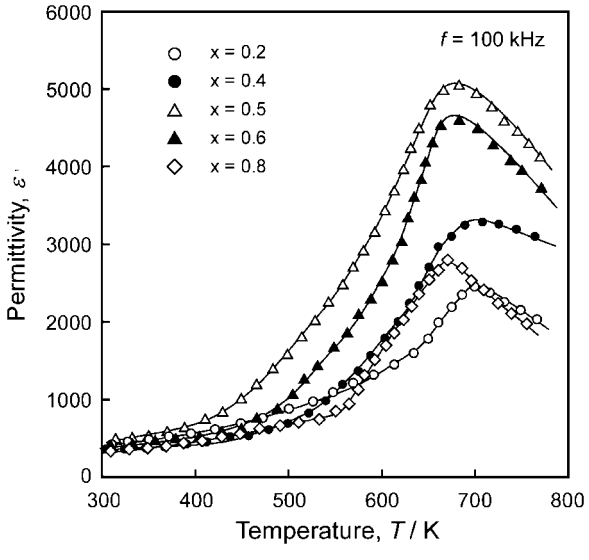

Fig. 8 Temperature dependence of permittivity for NKN films prepared on Pt/STO(100) substrates at $T_{sub} = 973\,K$, $P_{O_2} = 10\,Pa$ and $D_{t\text{-}s} = 60\,mm$ for 7.2 ks.

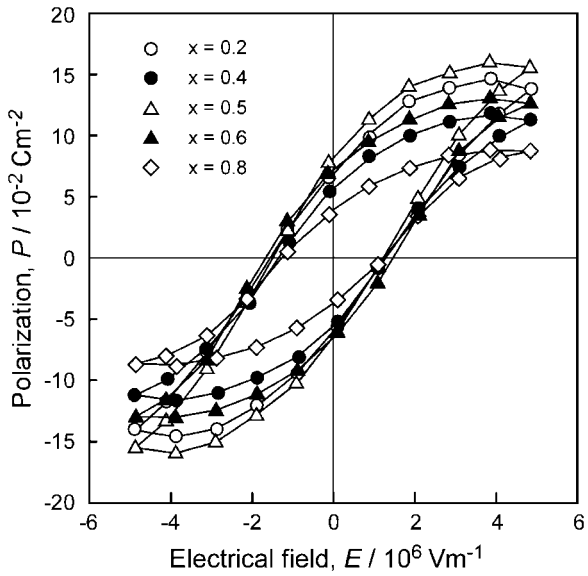

Fig. 9 Hysteresis loops of NKN films prepared on Pt/STO(100) substrates at $T_{sub} = 973\,K$, $P_{O_2} = 10\,Pa$ and $D_{t\text{-}s} = 60\,mm$ for 7.2 ks.

Table 2 Comparison of composition and permittivity values at 100 kHz of NKN films prepared by different methods.

$Na_xK_{1-x}NbO_3$	ε' at R.T.	ε' (Maximum) at T_c	Film deposition method	Ref.
$x = 0.5$	550	/	Pulsed laser deposition	10)
$x = 0.5$	200	/	Pulsed laser deposition	10)
$x = 0.5$	520	/	Magnetron sputtering	11)
$x = 0.5$	540	/	Sol-gel deposition	16)
$x = 0.5$	514	2500	Pulsed laser deposition	26)
$x = 0.5$	530	1200	RF magnetron sputtering	26)
$x = 0.5$	37	/	RF magnetron sputtering	28)
$x = 0.5$	545	/	Aerosol deposition	29)
$x = 0.5$	114	/	Pulsed laser deposition	30)
$x = 0.2$–0.8	390–520	5000 (at $x = 0.5$)	Pulsed laser deposition	This work

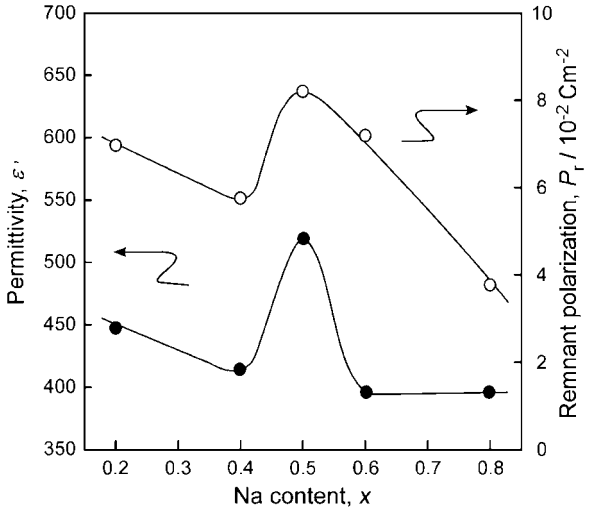

Fig. 10 Effect of x on permittivity at 100 kHz and remnant polarization at room temperature of NKN films prepared on Pt/STO(100).

4. Conclusions

NKN films with different compositions were prepared by pulsed laser deposition. The compositions of the films were almost the same as those of the targets. The lattice parameters of the deposited films were smaller than those of the targets. The NKN films had a dense, uniform granular microstructure. High T_{sub} and P_{O_2} promoted the (001) orientational growth. E_L was the key deposition parameter which controlled the particulate generation on the film surface. Permittivity and remnant polarization showed the maximum values of 520 and 8.2×10^{-2} C m^{-2} at 0.5NKN, while the highest permittivity value was 5000 at $T_c = 680$ K.

Acknowledgement

This research was partially supported by the Global COE Materials Integration Program, Tohoku University and the Japan Society for the Promotion of Science (JSPS), Asian CORE program "Interdisciplinary Science of Nanometers."

REFERENCES

1) K. Singh, V. Lingwal, S. C. Bhatt, N. S. Panwar and B. S. Semwal: Mater. Res. Bull. **36** (2001) 2365–2374.
2) V. Lingwal, B. S. Semwal and N. S. Panwar: Bull. Mater. Sci. **26** (2003) 619–625.
3) G. Shirane, R. Newnham and R. Pepinsky: Phys. Rev. **96** (1954) 581–588.
4) D. H. Cho, M. K. Ryu, S. S. Park, S. Y. Cho, J. G. Choi, M. S. Jang, J. P. Kim and C. R. Cho: J. Korean Phys. Soc. **46** (2005) 151–154.
5) B. P. Zhang, J. F. Li, K. Wang and H. L. Zhang: J. Am. Ceram. Soc. **89** (2006) 1605–1609.
6) R. E. Jaeger and L. Egerton: J. Am. Ceram. Soc. **45** (1962) 209–213.
7) Y. Saito, H. Takao, T. Tani, T. Nonoyama, K. Takatori, T. Homma, T. Nagaya and M. Nakamura: Nature **432** (2004) 84–87.
8) Y. Saito and H. Takao: Ferroelectrics **338** (2006) 1433–1448.
9) S. Abadei, S. Gevorgian, C.-R. Cho and A. Grishin: J. Appl. Phys. **91** (2002) 2267–2276.
10) C.-R. Cho and A. Grishin: J. Appl. Phys. **87** (2000) 4439–2228.
11) M. Blomqvist, J. H. Koh, S. Khartsev, A. Grishin and J. Andreasson: Appl. Phys. Lett. **81** (2002) 337–339.
12) H. J. Lee, C. W. Ahn, S. H. Kang, I. W. Kim, J. S. Lee and B. M. Jin: Ferroelectrics **335** (2006) 227–232.
13) C. R. Cho: Mater. Lett. **57** (2002) 781–786.
14) C. R. Cho and B. M. Moon: Integr. Ferroelectr. **45** (2002) 39–48.
15) F. Soderlind, P.-O. Kall and U. Helmersson: J. Cryst. Growth. **281** (2005) 468–474.
16) Y. Nakashima, W. Sakamoto, H. Maiwa, T. Shimura and T. Yogo: Jpn. J. Appl. Phys. Part 2 **46** (2007) L311–L313.
17) M. N. R. Ashfold, F. Claeyssens, G. M. Fuge and S. J. Henley: Chem. Soc. Rev. **33** (2004) 23–31.
18) C.-R. Cho and A. Grishin: Appl. Phys. Lett. **75** (1999) 268–270.
19) J.-S. Kim, I. R. Hwang, S. H. Hong, J. H. Lee, B. H. Park, A. C. Woo and N. Sahn: J. Korean Phys. Soc. **48** (2006) 1583–1587.
20) Y. T. Lu, X. M. Chen, D. Z. Jin and X. Hu: Mater. Res. Bull. **40** (2005) 1847–1855.
21) F. P. Lai and J. F. Li: J. Sol-Gel Sci. Technol. **42** (2007) 287–292.
22) A. Reisman and F. Holtzberg: J. Am. Ceram. Soc. **77** (1955) 2115–2119.
23) C. N. W. Darlington and H. D. Megaw: Acta Cryst. **B29** (1973) 2171–2177.
24) P. R. Guduru, E. Chason and L. B. Freund: J. Mech. Phys. Solid. **51** (2003) 2127–2148.
25) J. Bak-Misiuk, A. Misiuk, K. S. Zhuravlev, J. Z. Domagala, J. Adamczewska and V. V. Preobrazhenskii: Physica B **308–310** (2001) 820–822.
26) S. Khartsev, A. Grishin, J. Andreasson, J. H. Koh and J. S. Song: Integr. Ferroelectr. **55** (2003) 769–779.
27) S.-Y. Chu, W. Water, Y.-D. Juang and J.-T. Liaw: Ferroelectrics **287** (2003) 23–33.
28) V. M. Kugler, F. Soderlind, D. Music, U. Helmersson, J. Andreasson and T. Lindback: J. Cryst. Growth **254** (2003) 400–404.
29) J. Ryu, J.-J. Choi, B.-D. Hahn, D.-S. Park, W.-H. Yoon and K.-H. Kim: Appl. Phys. Lett. **90** (2007) 152901.
30) C. R. Cho, J. H. Koh, A. Grishin, S. Abadei and S. Gevorgian: Appl. Phys. Lett. **76** (2000) 1761–1763.